Laser and Particle Beams (2014), *32*, 359–367.

doi:10.1017/S0263034614000226

Langmuir probe studies of laser ablated ruby plasma and correlation with pulsed laser deposited ruby thin film properties

SATCHI KUMARI AND ALIKA KHARE

Laser and Photonics Laboratory, Department of Physics, Indian Institute of Technology Guwahati, Guwahati, India

(RECEIVED 28 December 2013; ACCEPTED 22 April 2014)

Abstract

In the present paper, measurement of various plasma parameters during pulsed laser deposition of ruby thin film on quartz substrate is reported. The variation of electron temperature and ion density with laser fluence and ambient pressure is recorded via Langmuir probe technique. The structural and optical properties of ruby thin films were analyzed using photo-luminescence and atomic force microscopy, and then correlated with the plasma parameters to find optimum conditions for deposition of high quality ruby thin film.

Keywords: Laser ablation; Langmuir probe; Ruby (Al_2O_3:Cr^{3+}); Thin film; Pulsed laser deposition

1. INTRODUCTION

Ruby (Al_2O_3:Cr^{3+}) has a wide range of applications in the field of optics and photonics, ranging from the first solid state laser to photonic temperature, stress and acoustic sensor (Maiman *et al*., 1960; Powell *et al*., 1998; Nelson *et al*., 1965; Cronemeyer *et al*., 1966; Ragan *et al*., 1992; Duan *et al*., 1997; Aizawa *et al*., 2002; Gibson *et al*., 1999). Recently, optical delay of light has also been demonstrated in ruby crystal and hence it can find application in quantum optics (Bigelow *et al*., 2003; Gao *et al*., 2008). In order to harness these properties of ruby in form of miniaturized device, the deposition of ruby thin film is reported by few researchers using solid phase epitaxy, electron beam deposition, and pulsed laser deposition (PLD) (Yu *et al*., 1995; Wen *et al*., 1995; Aizawa *et al*., 2009; Kumari *et al*., 2013). Among various techniques, PLD was found to be the most promising technique for deposition of epitaxial ruby thin film (Kumari *et al*., 2013; 2011). Moreover, PLD technique is found to be successful for deposition of high quality thin films of ceramic, heavy metals, and alloys (Sankur *et al*., 1986; Lorusso *et al*., 2011; Cracium *et al*., 1995; Mostako *et al*., 2012; Shukla *et al*., 2010). Also pulsed laser ablation is promising for nanoparticle synthesis (Wang *et al*., 2011), heavy ion generation and acceleration (Wolowski *et al*., 2007), and laser ablation lithography (Kamlesh *et al*., 2005; 2006). PLD is a versatile thin film deposition technique and it allows the control of thin film quality by varying various experimental parameters during deposition viz. laser fluence, gas pressure, etc. The quality of thin films deposited through PLD technique is governed by the properties of laser produced plasma. With the aim to investigate the properties of laser produced plasma as a function of laser fluence and gas pressure, a detailed study of the dynamics of the plasma species produced by laser ablation of ruby in oxygen environment during PLD is undertaken. The laser produced plasma parameters are investigated by recording ion and electron time of flight (TOF) signals using planar Langmuir probe. Further, an attempt is made to correlate the properties of the ruby thin films deposited by PLD to that of the laser induced plasma parameters.

2. EXPERIMENTAL SETUP

The experimental setup used for Langmuir probe study is shown in Figure 1. To produce the ruby plasma, second harmonic of a high power Nd:YAG Quanta Ray (model no: INDI-HG) ($\lambda = 532$ nm) laser was focused on to the ruby pellet using a plano convex lens of focal length 35 cm, placed inside a vacuum chamber. The Langmuir probe used in the experiment was in the form of a flat copper plate having dimension 4 mm × 4 mm, placed at a distance of 4 cm away from ruby target. The current-voltage I-V

Address correspondence and reprint requests to: Alika Khare, Laser and Photonics Laboratory, Department of Physics, Indian Institute of Technology Guwahati, Guwahati-781039, India. E-mail: alika@iitg.ernet.in

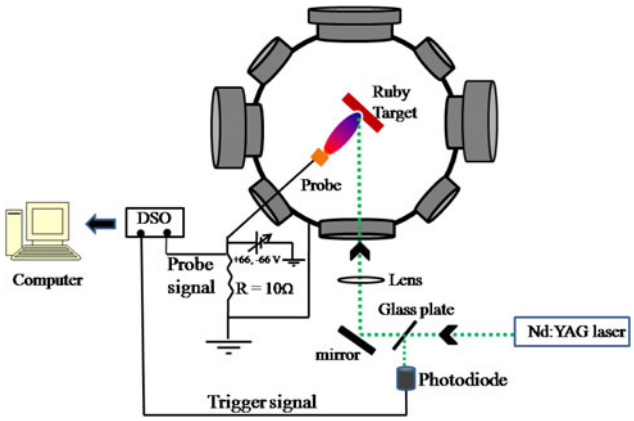

Fig. 1. (Color online) Schematic of experimental setup.

characteristics of Langmuir probe was recorded as a function of laser fluence and background gas pressure. To attend the I-V characteristics, the Langmuir probe biasing voltage was varied from +66 volt to −66 volt using the dual direct current regulated power supply (Testronix 93C). The electron and ion TOF signals were obtained by displaying the voltage drop across a 10 Ω ceramic resistor, connected toward the grounding end as shown in Figure 1, on a digital storage oscilloscope (DSO; Tektronix, DPO-3034) interfaced with a computer. The DSO was triggered with respect to the Nd:YAG laser pulse using a fast photodiode as shown in Figure 1. The signal pulses were averaged over 64 pulses. In order to deposit the thin films of ruby under the similar experimental conditions, the probe was replaced with the substrate holder assembly mounted at the same location. The PLD ruby thin film was deposited on quartz substrate, at a substrate temperature of 750°C for 1 hr. The ruby thin films were deposited at six different laser fluences ~6.2 J/cm^2, ~16 J/cm^2, ~23 J/cm^2, ~27 J/cm^2, and ~30 J/cm^2. In order to study the effect of oxygen gas pressure, the ruby thin films were deposited at five different gas pressure; ~0.05 mbar, ~0.1 mbar, ~1 mbar, ~5 mbar and ~10 mbar at a laser fluence of ~23 J/cm^2 for 1 hr.

3. RESULTS AND DISCUSSION

3.1. Effect of Laser Fluence on Plasma Parameters

The electron and ion TOF signal as a function of laser fluence at a bias voltage of ±60 volts is shown in Figure 2. It can be observed from the electron and ion TOF signal that the signal initially shows oscillatory behavior during the beginning of nanosecond Nd:YAG pulse. The oscillatory behavior observed in the initial part of electron and ion signals are associated with the ion plasma frequency and electron-ion collision frequency. These oscillations are induced by thermal fluctuations that appear in the plasma cooling process. These oscillations are explained in detail using a hydrodynamic model in a non-differentiable space-time (Nica *et al.*, 2010). The variation in oscillatory behavior with increase in laser fluence is due to increase in plasma density at higher laser fluences (Gurlui *et al.*, 2008). After the termination of pulse a fast peak of duration ~0.5 μs is observed followed by a broad slow peak of duration ~5 μs. The fast peak is the fast component of plasma originated due to photoelectrons accelerated via inverse bremsstrahlung processes. On the other hand, the broad peak (slow peak) in TOF curve actually corresponds to the arrival time of optimum ions/electrons flux to the probe. The electron/ion signals were found to increase on increasing the laser fluence from ~6.2 J/cm^2 to ~30 J/cm^2. The peak of the signal corresponding to the arrival time of species and was found to decrease from 5.3 μs to 3.7 μs in case of electron estimated using Figure 2a. In

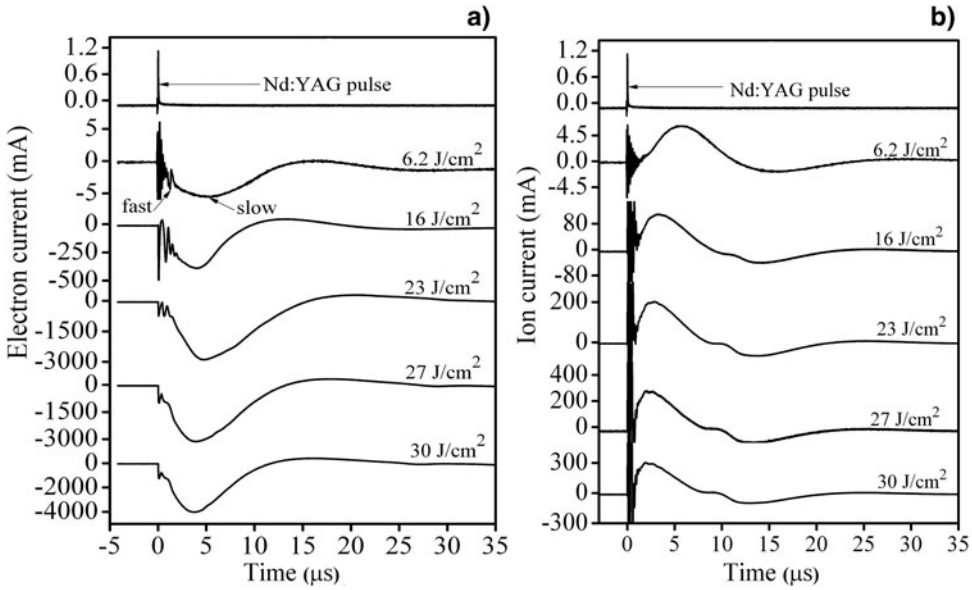

Fig. 2. (**a**) Electron TOF signals as a function of laser fluence (**b**) corresponding ion TOF signals.

https://doi.org/10.1017/S0263034614000226 Published online by Cambridge University Press

case of ion signal, the arrival time has been decreased from 5.7 μs to 2.2 μs, calculated from TOF signal of Figure 2b. Thus, the plasma species are reaching the probe surface in shorter time duration when increasing the laser fluence, due to conversion of thermal energy into kinetic energy. The electron current is observed to be larger than that of ion current at every laser fluence as observed from Figure 2a. The electron and ion velocities have been estimated using Eq. (1), and are shown in Figure 3.

$$v_i = d/t, \tag{1}$$

where v_i is the velocity of ion, d is the distance from target to probe, and t is the time taken by maximum number of ion to reach the probe surface. The electron velocity was found to increase from 31×10^5 cms^{-1} to 68×10^5 cms^{-1} in case of fast peak, on increasing the fluence from ~6.2 J/cm^2 to ~30 J/cm^2. In case of slow peak, similar behavior was observed. The electron velocity was found to vary from 10.0×10^5 cms^{-1} to 26×10^5 cms^{-1}. The ion velocity was also found to increase with increase in laser fluence. The ion velocity was found to increase from 7.0×10^5 cms^{-1} to 18×10^5 cms^{-1} on increasing the laser fluence from ~6.2 J/cm^2 to ~30 J/cm^2. The increase in electron/ion velocity with fluence is due to conversion of thermal energy into kinetic energy. The increase in velocities of both electrons as well as ions was slow up to ~23 J/cm^2 but beyond that it has increased drastically. The I-V characteristics of Langmuir probe at various laser fluence are shown in Figure 4. The electron and ion current is clearly shown to increase with increase in laser fluence. The inset of Figure 4 shows a semi-logarithmic plot of the I-V curve for the laser fluence of ~30 J/cm^2. The data points for bias voltage of 0 to 10 volts, taken at a step of 1 volt is linear fitted.

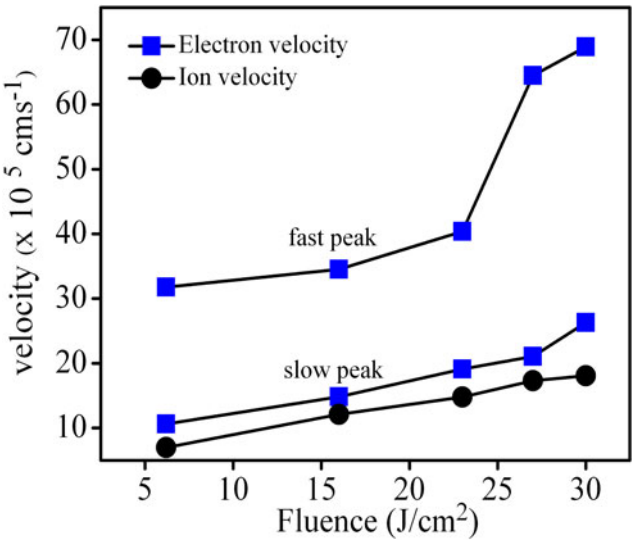

Fig. 3. (Color online) Electron and ion velocities at various fluences.

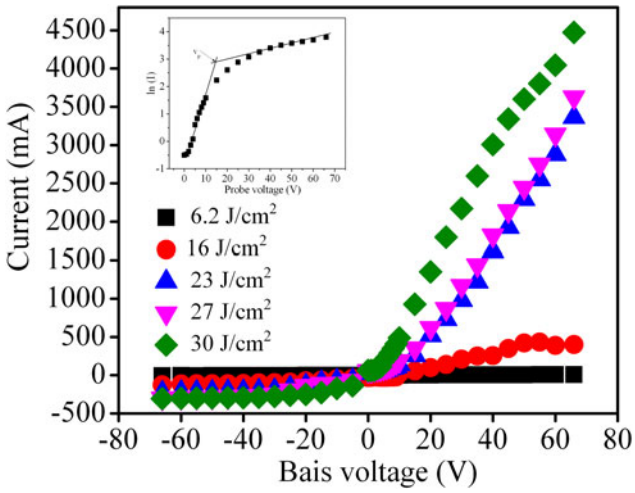

Fig. 4. (Color online) I-V characteristics at various laser fluences.

The slope of the curve ln (I_p) vs. V, given by

$$\frac{d \ln (I_P)}{dV} = \frac{1}{T_e} \tag{2}$$

gives the value of electron temperature in eV. The ion density was calculated by

$$I_i = Aenv_i \tag{3}$$

where I_i is the saturation current for ion, A is the area of probe, and v_i is the velocity of ion.

The electron temperature and ion density as a function of laser fluence is shown in Figure 5. The electron temperature was found to increase from 0.5 eV to 3.2 eV on increasing the laser fluence as shown in Figure 5a. The error in the estimation of electron temperature was in the range 0.15 eV to 0.18 eV as shown in the Figure 5a. The ion density was also found to increase from 3.6×10^{12} cm^{-3} to 6.8×10^{12} cm^{-3} with increase in fluence from ~6.2 J/cm^2 to ~30 J/cm^2. The plasma temperature and density was found to increase rapidly up to a laser fluence of ~23 J/cm^2. Beyond ~23 J/cm^2, the plasma temperature and density shows steady increase and almost close to saturation. This could be due to formation of self-regulating regime near the target surface at high laser fluence (Harilal *et al.*, 1997). If the absorption of the laser photons by the plasma becomes higher due to high plasma density, the evaporation of the species from the target becomes less, which in turn decreases density of the charged species. This consequently increases the absorption of the laser photons by the target, thus increasing the temperature of the plasma.

3.2. Effect of Gas Pressure Variation

The gas pressure was varied from ~10^{-5} mbar to ~10 mbar. Figure 6 shows the electron and ion TOF signals,

https://doi.org/10.1017/S0263034614000226 Published online by Cambridge University Press

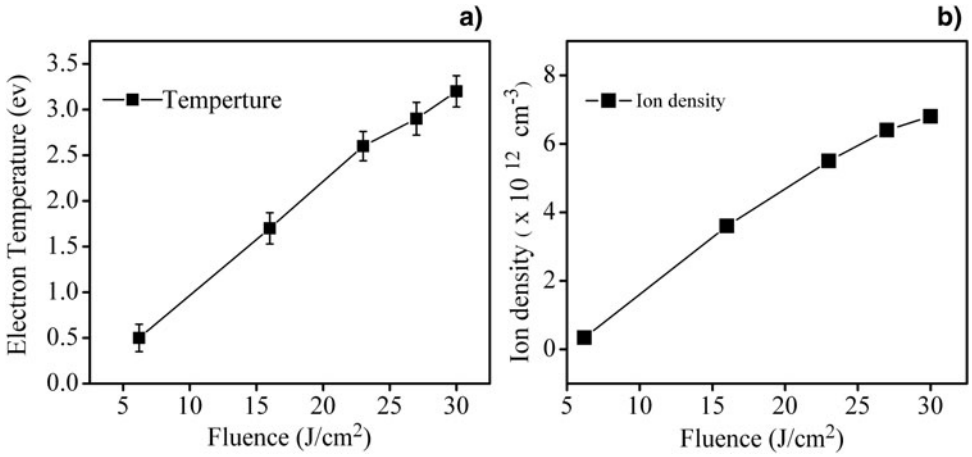

Fig. 5. Variation of (**a**) plasma temperature and (**b**) ion density as a function of laser fluence.

respectively, as a function of background gas pressure. With increase in gas pressure the electron current has been drastically reduced. The ion TOF signal also shows similar kind of behavior as shown in Figure 6b. The ion collection by the probe was very large in vacuum but with increase in gas pressure it has reduced drastically. The reduction in electron/ion current with increase in background gas pressure could be due to loss of charged species on collision with gas molecules. Moreover, the collision rate will further increase due to confinement of plasma with increase in gas pressure. This will further lead to reduction in electron/ion current. The electron and ion velocities estimated from the electron and ion TOF signals of Figure 6 using Eq. (1), is shown in Figure 7. The electron velocity for fast peak was found to decrease from 64×10^5 cms^{-1} to 25×10^5 cms^{-1} with increase in pressure from 10^{-5} mbar to 10 mbar. In case of slow peak, it is nearly constant up to 10^{-1} mbar of oxygen pressure and then it increased from 11.7×10^5 cms^{-1} to 30.3×10^5 cms^{-1} up to ~5 mbar, and then reduced to 13.2×10^5 cms^{-1} at ~10 mbar. The ion velocity was increased from 9.7×10^5 cms^{-1} to 22.2×10^5 cms^{-1}, with increase in oxygen pressure from ~10^{-5} mbar to ~10^{-1} mbar, and then decreased to 17.3×10^5 cms^{-1} on further increasing the pressure to 10 mbar. The I − V characteristics as a function of gas pressure are shown in Figure 8. The electron temperature and ion density as a function of oxygen gas pressure is estimated using Eqs. (2) and (3), respectively, and is shown in Figure 9. The electron temperature initially increases from 0.8 eV to 3.8 eV, on increasing the pressure from ~10^{-5} mbar to ~0.05 mbar. On further increasing the

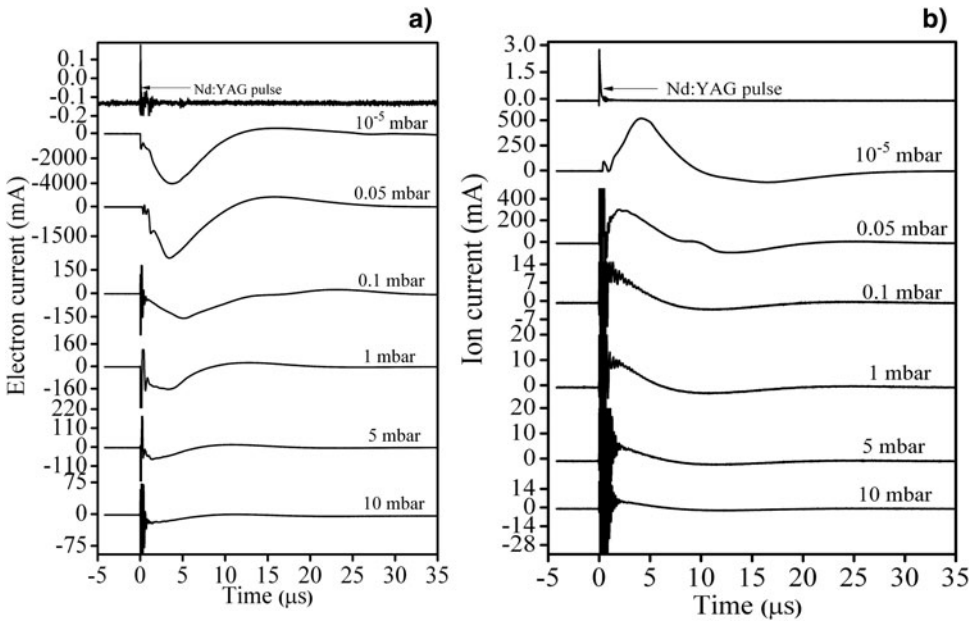

Fig. 6. (**a**) Electron TOF signals as a function of gas pressure (**b**) corresponding ion TOF signals.

https://doi.org/10.1017/S0263034614000226 Published online by Cambridge University Press

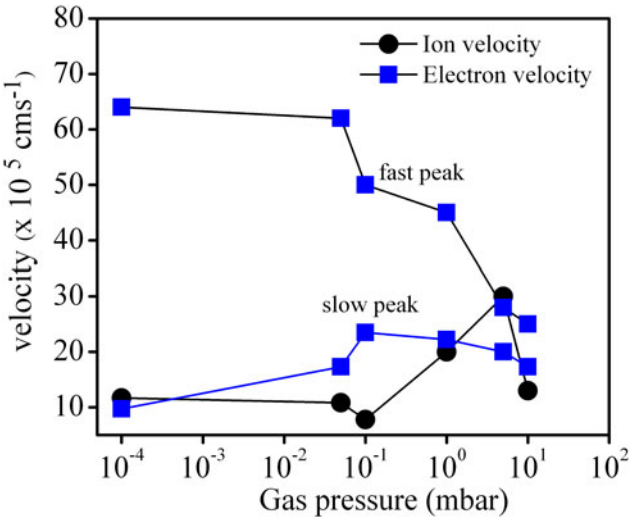

Fig. 7. (Color online) Electron and ion velocities as a function of gas pressure.

pressure from 0.1 mbar to 10 mbar the electron temperature was found to reduce from 2.5 eV to 0.5 eV as shown in Figure 9a. The error in the estimation of electron temperature is in the range of 0.11 to 0.15 eV. The ion density has been found to reduce from 2.1×10^{12} cm^{-3} to 6.2×10^{10} cm^{-3}, on increasing the gas pressure from 10^{-5} mbar to 10 mbar. The observed behavior in electron temperature and ion density as a function of gas pressure can be explained on the basis of plasma confinement. As the pressure increases, the confinement of the plasma takes place near the target surface (Harilal *et al.*, 1998) this results in the increase in the electron collision rate with the background gas atoms. Energy loss due to elastic collision supersedes the rate of growth of energy of free electrons via inverse bremsstrahlung processes. Thus the temperature & ion density reduces with increase in background gas pressure.

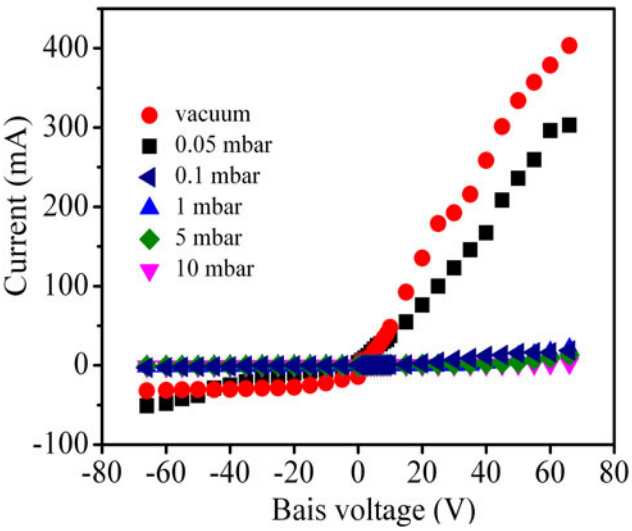

Fig. 8. (Color online) I-V characteristics as a function of gas pressure.

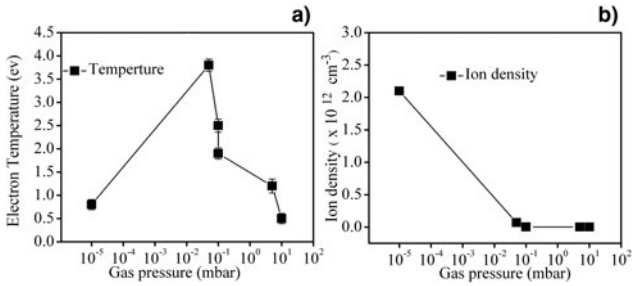

Fig. 9. Variation of (**a**) plasma temperature and (**b**) ion density as a function of gas pressure.

3.3. PLD of Ruby Thin Film and Correlation with Plasma Parameters

3.3.1. Effect of Laser Fluence

To monitor the effect of laser fluence onto the quality of PLD deposited ruby thin films the films were deposited at six laser fluences; ~2 J/cm^2, ~6.2 J/cm^2, ~16 J/cm^2, ~23 J/cm^2, and ~30 J/cm^2. The thickness of the film was found to increase from 15 nm to 185 nm on increasing the laser fluence from ~2 J/cm^2 to ~23 J/cm^2 as shown in Figure 10a. On further increasing the laser fluence to ~27 J/cm^2 and ~30 J/cm^2 the thicknesses drops down to 150 nm and 120 nm, respectively. The photo-luminescence (PL) intensity of films also scales with the increase in laser fluences as shown in Figure 10b. At low laser energy ~2 J/cm^2 and ~6.2 J/cm^2 the PL spectra does not show any signature of ruby phase in the deposited film as shown in inset of Figure 10b. On increasing the laser fluence to ~16 J/cm^2, distinct R_1 and R_2 lines at 692.8 nm and 694.2 nm is observed in the PL spectra, confirming the ruby phase in the film. On increasing the laser energy to ~23 J/cm^2, drastic enhancement in PL intensity is observed. The atomic force microscopy (AFM) images of PLD ruby thin films are shown in Figure 11. The surface roughness and average grain size estimated using the micrographs of Figure 11 are listed in Table 1. It shows decrease in surface roughness from 6.0 nm to 3.0 nm on increasing the laser fluence from ~2 J/cm^2 to ~23 J/cm^2. The surface roughness is increased to 4.6 nm at a fluence of ~30 J/cm^2. The grain size has been increased from 40.5 nm to 54.6 nm with increase in laser fluence. At higher laser fluence more particles are ejected from the target surface. Thus, the kinetic energy as well as amount of target species arriving onto the substrate surface increases with increases in laser fluence. On arriving the surface of the substrate these particles accumulates to form a larger grain in order to minimize their surface energy (Lorusso *et al.*, 2011). Thus, higher laser fluence gives rise to a thicker film as shown in Figure 10a. At high laser fluence the kinetic energy of ablated material is high which results in good adhesion of the film onto the substrate as well as the formation of crystalline structure. The improved crystalline structure of the film promotes the better surface-atom mobility (Cracium *et al.*, 1995). Thus, the PL signal is improved at higher laser fluences as observed from Figure 10b. As the laser fluence was

https://doi.org/10.1017/S0263034614000226 Published online by Cambridge University Press

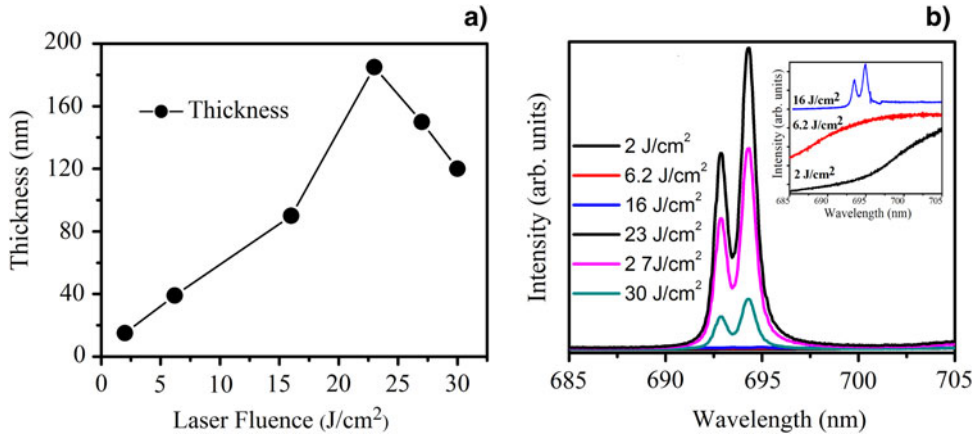

Fig. 10. (Color online) (**a**) Thickness and (**b**) photoluminescence of PLD deposited ruby thin film as a function of laser fluence.

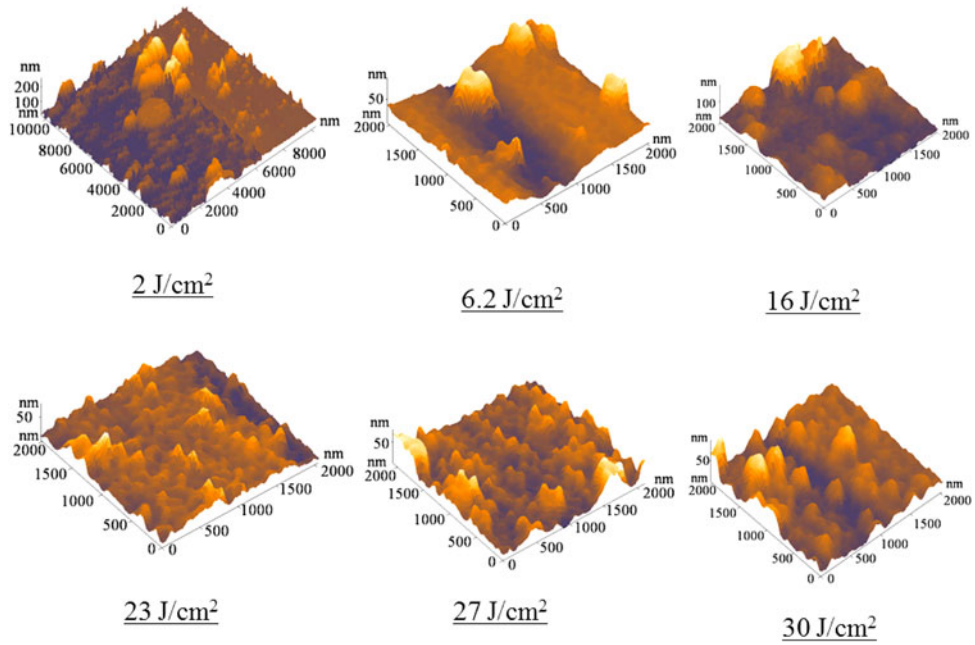

Fig. 11. (Color online) AFM images of PLD ruby thin film as a function of laser fluences.

Table 1. *List of PLD ruby thin films deposited at various laser fluences*

Laser fluence (J/cm^2)	Deposition time (hour)	Gas pressure (mbar)	Thickness (nm)	Deposition Rate (nm/min)	Grain size (nm)	Roughness (nm)
2.0	1	0.05	15	0.25	40.5	6.0
6.2	1	0.05	39	0.65	45.0	6.2
16.0	1	0.05	90	1.50	55.2	4.5
23.0	1	0.05	185	3.08	50.4	2.6
27.0	1	0.05	150	2.50	52.6	3.2
30.0	1	0.05	120	2.00	54.6	4.6

further increased to ~27 J/cm^2 and ~30 J/cm^2 the PL intensity was found to decrease. This could be due to sputtering from the film surface on impingement of highly energetic particle on substrate surface. The increase in surface roughness at these laser fluences further suggest that there could be sputtering from film surface.

https://doi.org/10.1017/S0263034614000226 Published online by Cambridge University Press

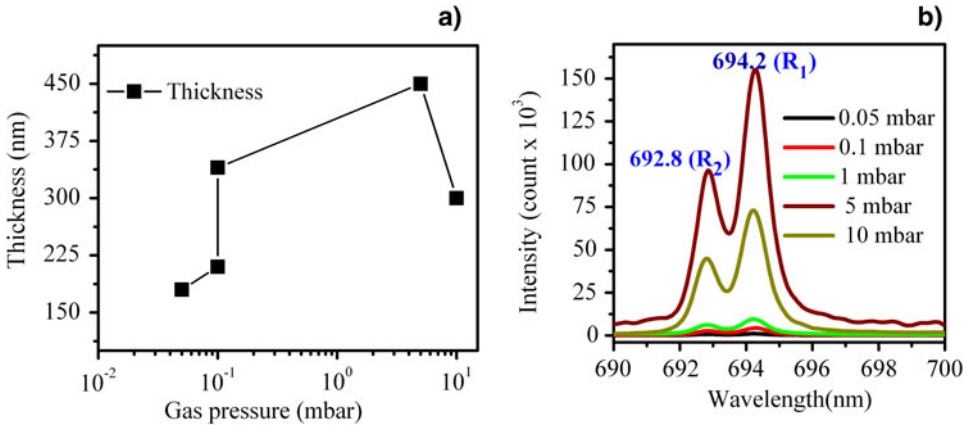

Fig. 12. (Color online) (**a**) Thickness and (**b**) photoluminescence of PLD deposited ruby thin film as a function of gas pressure.

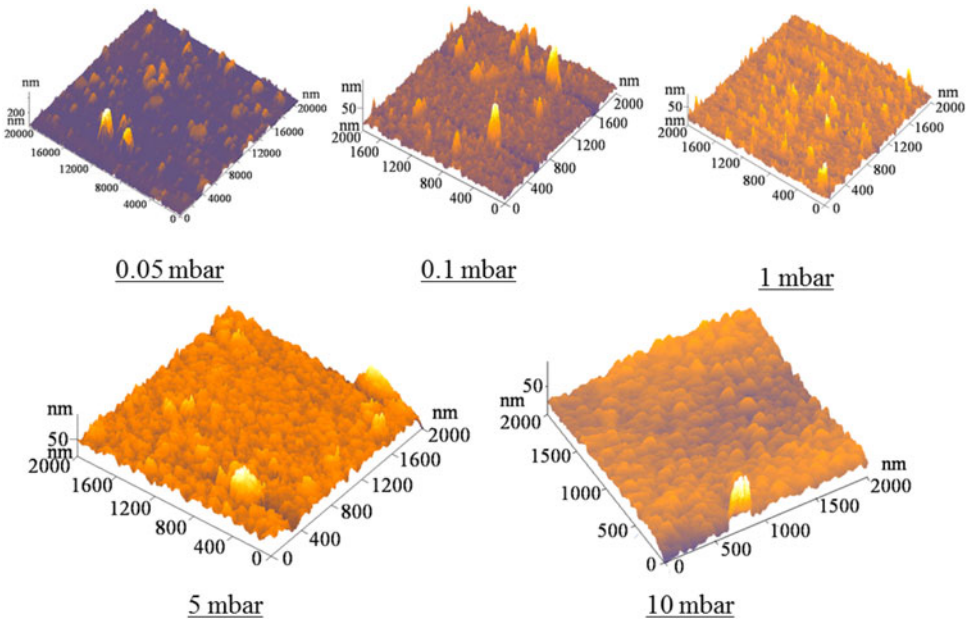

Fig. 13. (Color online) AFM images of PLD ruby thin film as a function of gas pressure.

Thus, the optimum laser fluence for deposition of ruby thin film is ~23 J/cm^2. Above this laser fluence the ion and electron velocity has drastically increased, as observed from Figure 3. Due to rapid increase in the velocity of plasma species, sputtering from the film surface takes place on impingement of these highly energetic particles. Thus, the quality of film has been deteriorated as reflected from increase in the surface roughness and decrease in PL intensity of ruby thin films deposited at laser fluence of ~27 J/cm^2 and ~30 J/cm^2.

3.3.2. Effect of Gas Pressure

To attain the optimum oxygen pressure for deposition of PLD ruby thin films, the films were deposited at five different oxygen gas pressures ~0.05 mbar, ~0.1 mbar, ~1 mbar, ~5 mbar, and ~10 mbar. Figure 12a shows the thickness of PLD ruby thin film as a function of background gas pressure. The thickness of the film was found to increase from 180 nm to 450 nm on increasing the gas pressure from ~0.05 mbar to ~5 mbar, on further increasing the gas pressure to 10 mbar the thickness was found to decrease to a value of 300 nm. The PL spectra as shown in Figure 12b, shows increase in PL intensity up to ~5 mbar and then drastically fall at 10 mbar. Figure 13 shows the AFM micrographs of ruby thin film grown under various oxygen pressures and the estimated surface roughness and average grain size are listed in Table 2. With increase in oxygen pressure from 0.05 mbar to 10 mbar, the surface roughness was found to increase from 2.0 nm to 5.9 nm. Whereas, the grain size was found to increase from 55.5 nm to 120 nm, with increase in gas pressure from ~0.05 mbar to ~10 mbar. Initially, with the increase in gas pressure from ~0.05 mbar to ~5 mbar, expansion of

https://doi.org/10.1017/S0263034614000226 Published online by Cambridge University Press

Table 2. *List of PLD ruby thin films deposited at various gas pressures*

Gas pressure (mbar)	Deposition time (hr)	Laser fluence (J/cm^2)	Thickness (nm)	Deposition Rate (nm/min)	Grain size (nm)	Roughness (nm)
0.05	1	23.0	180	3.00	55.50	2.05
0.1	1	23.0	210	3.50	62.90	2.97
1	1	23.0	340	5.67	95.21	3.80
5	1	23.0	450	7.50	105.00	5.48
10	1	23.0	300	5.00	120.00	5.92

plasma plume is confined. The losses of plasma species due to scattering is reduced and density increases and hence the thickness of the film increases as observed from Figure 12a. The increase in PL intensity is also in accordance with the thickness result. With further increase in pressure to ~10 mbar the plasma is confined in a very small region as well as due to increase in collisions forward movement of the plasma towards the substrate is curtailed leading to the decrease in deposition rate (Wang *et al*., 2005). Thus, the thickness as well as PL intensity has been reduced as observed from Figure 12. Thus, the optimum gas pressure could be ~5 mbar for deposition of ruby thin film.

4. CONCLUSION

In this paper, Langmuir probe investigation of ruby plasma during pulsed laser deposition of ruby thin film in oxygen ambient is reported. The dependence of electron temperature and ion density as a function of laser fluence and oxygen pressure was studied. Structural and optical characterization of ruby thin films revealed that with increase in laser fluence the quality of film was improved. But at very high laser fluence the quality of film is degraded due to very high kinetic energy of ablated species supporting the Langmuir probe studies. The optimum laser fluence was found to be ~23 J/cm^2. Increasing the gas pressure resulted in increase in film thickness due to plasma confinement as evident from plasma studies. At very high gas pressure over confinement of plasma curtailed the forward motion of species resulting in lower deposition rate. Oxygen pressure ~5 mbar was found to be optimum gas pressure for PLD deposition of ruby thin film.

ACKNOWLEDGEMENT

This work was supported in part by Department of science and technology Govt. of India Grant no. SR/S2/HEP-0019/2008.

REFERENCES

Aizawa, H., Ohishi, N., Ogawa, S., Katsumata, T. & Komuro, S. (2002). Fabrication of ruby sensor probe for the fiber-optic thermometer using fluorescence decay. *Rev. Sci. Instrum.* **73**, 3656–3658.

Aizawa, H., Shibasaki, M., Komuro, S., Miyazaki, Y. & Katsumata, T. (2009). Fabrication of ruby thin film for temperature indicator application. International Conference on Electrical Engineering.

Bigelow, M.S., Lepeshkin, N.N. & Boyd, R.W. (2003). Observation of ultraslow light propagation in a ruby crystal at room temperature. *Phy. Rev. Lett.* **90**, 1139031.

Cronemeyer, D.C. (1966). Optical absorption characteristics of pink ruby. *J. Opt. Soc. Am.* **56**, 1703–1706.

Cracium, V., Amirhaghi, S., Cracium, D., Elders, J., Gardeniers, J.G.E. & Boyd, I.W. (1995). Effects of laser wavelength and fluence on the growth of ZnO thin films by pulsed laser deposition. *Appl. Surf. Sci.* **86**, 99–106.

Duan, W., Paiva, Renata M., Wentzcovitch, M. & Fazzio, A. (1997). Ruby's optical transitions: effects of pressure-induced phase transformation. *Mat. Res. Soc. Symp. Proc.* **499**, 275.

Gibson, U.J. & Chernuschenko, M. (1999). Ruby films as surface temperature and pressure sensors. *Opt. Express* **4**, 443–448.

Gao, F., Xu, J., Zhang, G., Bo, F. & Liu, H. (2008). Paraxial energy transport of a focused Gaussian beam in ruby with nondegenerate two-wave coupling like mechanism. *Appl. Phys. Lett.* **92**, 021121.

Gurlui, S., Agop, M., Nica, P., Ziskind, M. & Focsa, C. (2008). Experimental and theoretical investigation of a laser-produced aluminum plasma. *Phys. Rev. E* **78**, 026405.

Harilal, S.S., Bindhu, C.V., Issac, R.C., Nampoori, V.P.N. & Vallabhan, C.P.G. (1997). Electron density and temperature measurement in a laser produced carbon plasma. *J. Appl. Phys.* **82**, 2140–2146.

Harilal, S.S., Bindhu, C.V., Nampoori, V.P.N. & Vallabhan, C.P.G. (1998). Influence of ambient gas on the temperature and density of laser produced carbon plasma. *Appl. Phys. Lett.* **72**,167–169.

Kumari, S. & Khare, A. (2013). Optical and structural characterization of pulsed laser deposited ruby thin films for temperature sensing application. *Appl. Surf. Sci.* **265**, 180.

Kumari, S. & Khare, A. (2011). Epitaxial ruby thin film based photonic sensor for temperature measurement. *Rev. Sci. Instrum.* **82**, 066106.

Kamlesh, A. & Khare, A. (2005). Low-energy low-divergence pulsed indium atomic beam by laser ablation. *Laser Part. Beams* **24**, 47.

Kamlesh, A. & Khare, A. (2006). Sculpted pulsed indium atomic beams via selective laser ablation of thin film. *Laser Part. Beams* **24**, 469.

Lorusso, A., Fasano, V., Perrone, A. & Lovchinov, K. (2001). Y thin films grown by pulsed laser ablation. *J. Vac. Sci. Technol. A* **29**, 031502.

Maiman, T.H. (1960). Stimulated optical radiation in ruby. *Nat.* **187**, 493.

Mostako, A.T.T. & Khare, A. (2012). Molybdenum thin films via pulsed laser deposition technique for first mirror application. *Laser Part. Beams* **30**, 559–567.

Nelson, D.F. & Sturge, M.D. (1965). Relation between absorption and emission in the region of the R lines of ruby. *Phy. Rev. A* **137**, 1117.

Nica, P., Agop, M., Gurlui, S. & Focsa, C. (2010). Oscillatory Langmuir probe ion current in laser-produced plasma expansion. *EPL* **89**, 65001.

Powell, R.C. (1998). *Physics of Solid State Laser Engineering*. Washington, DC: AIP Press.

Ragan, D.D., Gustavsen, R. & Schiferl, D. (1992). Calibration of the ruby R1 and R2 fluorescence shifts as a function of temperature from 0 to 600 K. *J. Appl. Phys.* **72**, 5539–5544.

Shukla, G. & Khare, A. (2010). Spectroscopic studies of laser ablated ZnO plasma and correlation with pulsed laser deposited ZnO thin film properties. *Laser Part. Beams* **28**, 149–155.

Sankur, H. (1986). Properties of thin PbF2 films deposited by cw and pulsed laser assisted evaporation. *Appl. Opt.* **25**, 1962–1965.

Yu, N., Wen, Q., Clarke, D.R., Mclntyre, P.C., Kung, H., Nastasi, M., Simpson, T.W., Mitchell, I.V. & Li, D. (1995). Formation of iron or chromium doped epitaxial sapphire thin films on sapphire substrates. *J. Appl. Phys.* **78**, 5412–5421.

Wen, Q., Clarke, D.R., Yu, N. & Nastasi, M. (1995). Epitaxial regrowth of ruby on sapphire for an integrated thin film stress sensor. *Appl. Phys. Lett.* **66**, 293–295.

Wang, Y.L., Chen, C., Ding, X.C., Chu, L.Z., Deng, Z.C., Liang, W.H., Chen, J.Z. & FU, G.S. (2011). Nucleation and growth of nanoparticles during pulsed laser deposition in an ambient gas. *Laser Part. Beams* **29**, 105–111.

Wolowski, J., Badziak, J., Czarnecka, A., Parys, P., Pisarek, M., Rosinski, Turan R. & Yerci, S. (2007). Application of pulsed laser deposition and laser-induced ion implantation for formation of semiconductor nano-crystallites. *Laser Part. Beams* **25**, 65–69.

Wang, C., Cheng, B.L., Wang, S.Y., Lu, H.B., Zhou, Y.L., Chen, Z.H. & Yang, G.Z. (2005). Effects of oxygen pressure on lattice parameter, orientation, surface morphology and deposition rate of (Ba0.02Sr0.98)TiO3 thin films grown on MgO substrate by pulsed laser deposition. *Thin Solid Films* **485**, 82–89.